

Research Article www.acsami.org

Closed-Loop Controlled Photopolymerization of Hydrogels

Manjot Singh, Junru Zhang, Keturah Bethel, Yang Liu, Eric M. Davis, Haibo Zeng, Zhenyu Kong, and Blake N. Johnson*



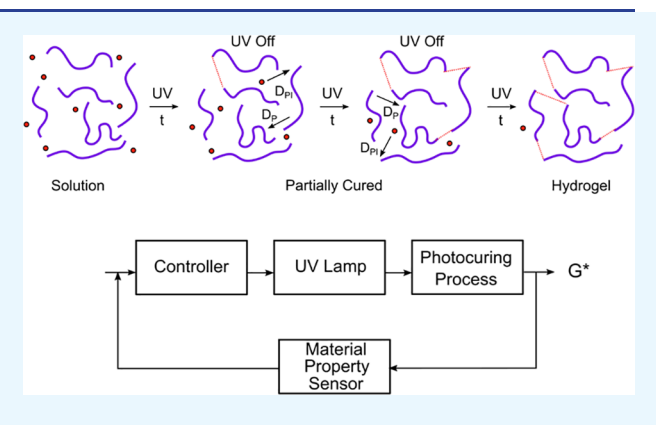
Cite This: ACS Appl. Mater. Interfaces 2021, 13, 40365-40378



ACCESS |

III Metrics & More

ABSTRACT: Here, we present a closed-loop controlled photopolymerization process for fabrication of hydrogels with controlled storage moduli. Hydrogel crosslinking was associated with a significant change in the phase angle of a piezoelectric cantilever sensor and established the timescale of the photopolymerization process. The composition, structure, and mechanical properties of the fabricated hydrogels were characterized using Raman spectroscopy, scanning electron microscopy (SEM), and dynamic mechanical analysis (DMA). We found that the storage moduli of photocured poly(ethylene glycol) dimethacrylate (PEGDMA) and poly(Nisopropylacrylamide) (PNIPAm) hydrogels could be controlled using bang-bang and fuzzy logic controllers. Bang-bang controlled photopolymerization resulted in constant overshoot of the storage modulus setpoint for PEGDMA hydrogels, which was mitigated by



Article Recommendations

setpoint correction and fuzzy logic control. SEM and DMA studies showed that the network structure and storage modulus of PEGDMA hydrogels were dependent on the cure time and temporal profile of UV exposure during photopolymerization. This work provides an advance in pulsed and continuous photopolymerization processes for hydrogel engineering based on closed-loop control that enables reproducible fabrication of hydrogels with controlled mechanical properties.

KEYWORDS: crosslinking, UV curing, photocuring, mechanical properties, rheological properties, closed-loop control

1. INTRODUCTION

Hydrogels are used in multiple applications, including tissue engineering, drug delivery, and energy storage. 1-6 Hydrogels can be formed using an assortment of crosslinking chemistries, including physical entanglement of polymers, entanglement of ionic-covalent networks, and free radical-initiated polymerization.^{7,8} Photocurable hydrogels formed through photoinitiated crosslinking reactions are attractive systems given their ease of processability and compatibility with synthetic and natural polymers. For example, photocurable hydrogels can rapidly solidify without temperature change or chemical exposure, making them attractive candidates for tissue engineering applications. The mechanical properties of hydrogel scaffolds, such as photocurable hydrogel scaffolds, are highly correlated with functional outcomes and utility of engineered tissues. 9-12 Parekh et al. showed that increasing the modulus of hydrogel scaffolds from 0.5 kPa to 59 kPa enhanced the osteogenic differentiation of human bone marrow stromal cells. 12 Wang et al. reported that human mesenchymal stem cells expressed more neurogenic protein markers on soft hydrogel substrates (0.6 kPa), while cells on relatively more stiff hydrogel substrates (12 kPa) exhibited an up-regulation of myogenic protein markers with varying morphologies and proliferation rates. 13

Hydrogels are typically formed using open-loop crosslinking processes that lack the ability to monitor and control the extent of reaction and the resultant structure and properties. While useful in various research applications, open-loop photopolymerization processes limit the achievable material quality and reproducibility, which are paramount in many applications (e.g., tissue engineering). For example, open-loop photopolymerization processes limit control over the extent of reaction, the rate of the crosslinking reaction, and thus, resultant material properties. Open-loop photopolymerization processes that lack real-time monitoring capabilities can also result in over- and underexposure effects. For example, the extent of UV exposure was shown to affect the mechanical properties, swelling, and wettability of PEGDMA hydrogels cured based on comparison among hydrogels fabricated using chamber-based curing vs. stereolithography. 14 Overexposure to

June 23, 2021 Received: Accepted: August 10, 2021 Published: August 20, 2021





UV light may also affect the components of engineered tissues, such as cells and proteins, by reaction with free radicals. 15,16

Traditionally, the properties of hydrogels cured using openloop (continuous exposure) photopolymerization have been controlled through the material formulation, such as the concentration of monomers and photoinitiators. Thus, the properties and reproducibility of materials produced using open-loop (continuous exposure) photopolymerization were dependent on the fidelity of the reagents and consistency in material preparation. Further, such traditional processes lack online monitoring of the extent of reaction or material properties. The identified limitations associated with openloop polymer curing processes have led to novel closed-loop controlled material curing processes. For example, Genidy et al. created a closed-loop feedback system for the determination of cure cycles that reduced cure shrinkage stresses in thermosetting polymer composites.¹⁷ In that study, a closedloop feedback controller was used to adjust the heating rate during the curing process to minimize the force on the embedded fiber induced by unrelaxed stress in the material. Kurtz et al. developed a multivariable nonlinear feedback controller for free-radical polymerization of methyl methacrylate by controlling the monomer concentration and reactor temperature.¹⁸ Zhao and Rosen created an approach for feedback control of a cured part's height using a projection lithography process based on real-time interferometry. 19 These studies suggest that the integration of real-time material property sensing with traditional open-cast photopolymerization processes could enable the reproducible fabrication of a range of hydrogel-based products, such as engineered tissues.

Given their ability to serve as measures of processability and performance across various applications, 9-12 the mechanical properties of hydrogels are important process parameters and quality measures in hydrogel processing. Here, we present a novel closed-loop controlled photopolymerization process based on real-time sensing of the hydrogel storage modulus. The performance of the closed-loop controlled photopolymerization process is examined using multiple control system designs and two hydrogel systems, poly(ethylene glycol) dimethacrylate (PEGDMA) and poly(N-isopropylacrylamide) (PNIPAm). Poly(ethylene glycol) (PEG) and PEG-based hydrogels (e.g., PEGDMA) have been extensively explored as cell scaffolds because of their hydrophilicity, biocompatibility, resistance to protein adsorption, and cell adhesion.²⁰⁻ PNIPAm hydrogels are stimuli-responsive systems, known for their mechanical response to thermal stimuli. Composite PEGand PNIPAm-based hydrogels are currently being examined as dual thermo- and photoresponsive materials for various applications. ^{24,25} A comparison of bang-bang and fuzzy logic controlled photopolymerization processes is made in terms of the achievable cure rate and extent of setpoint (storage modulus) overshooting. A comparison of various bang-bang controllers is provided in terms of the achievable cure rate, extent of setpoint overshooting, and final mechanical properties of resultant materials. Thus, we investigate the ability to control the mechanical properties of a photocurable hydrogel and demonstrate that the cure rate and temporal profile of UV light exposure can affect the structure and properties of PEGDMA hydrogels.

2. EXPERIMENTAL SECTION

2.1. Materials. Poly(ethylene glycol) dimethacrylate (PEGDMA) (750 Da), *N*-isopropylacrylamide (NIPAm) (113.16 g/mol), *N*,*N*′-

methylenebis(acrylamide) (MBA; 154.17 g/mol), and 2,2-dimethoxy-2-phenylacetophenone (DMPA) (256.30 g/mol) were purchased from Sigma-Aldrich. Lead zirconate titanate (PZT-5A; $72.4 \times 72.4 \times 0.127 \text{ mm}^3$) with nickel electrodes was from Piezo Systems, Inc. (Woburn, MA). Glass cylinders and ethanol (200 proof) were from Fisher Scientific. Polyurethane (Fast-Drying) was from Minwax. Epoxy (EA 1C-LV) and cyanoacrylate (409 Super Bonder) were from Loctite.

2.2. Hydrogel Precursor Preparation. PEGDMA precursor solutions (8, 10, and 12 wt %) were prepared by dissolving PEGDMA in deionized water (DIW). NIPAm precursor solutions (8, 10, and 12 wt %) were prepared by dissolving 0.5 g of NIPAm and 0.5 g of 1% MBA in DIW, with 5.25, 4, or 3.17 g of DIW to make 8, 10, or 12 wt %, respectively. A total of 0.2% of 20 wt % DMPA in ethanol was used as the photoinitiator.

2.3. Fabrication of Piezoelectric-Excited Millimeter Cantilever Sensors. Piezoelectric-excited millimeter cantilever (PEMC) sensors were fabricated from lead zirconate titanate (PZT) as described in a previous study.²⁶ Briefly, PZT sheets were diced into chips $(2 \times 1 \times 0.16 \text{ mm}^3 \text{ and } 5 \times 1 \times 0.127 \text{ mm}^3$, respectively; American Dicing; Liverpool, NY). Top and bottom faces of PZT were soldered to 30-gauge copper (Cu) wires of the nickel electrodes on the distal end. The cantilever was then potted in a glass cylinder (6 mm in diameter) with a nonconductive epoxy, resulting in a cantilever geometry $(3 \times 1 \times 0.127 \text{ mm}^3)$. Additional epoxy was applied on one side of PZT to create an asymmetric anchor. The sensors were then coated with polyurethane via spin coating (1000 rpm for 2 min), which was then allowed to cure at room temperature to improve the adhesion of parylene C to the sensor. The sensors were then coated with parylene C (10 μ m-thick) following vendor protocols (PDS 2010 Labcoter; Specialty Coating Systems; Indianapolis, IN). Following parylene C coating, the sensors were annealed for 1 h at 75 °C.

2.4. Measurement Principle and Data Acquisition. The resonant frequency (f_n) , phase angle at resonance (ϕ_n) , and impedance (Z_n) at resonance of the sensor, where n indicates the mode number, were continuously monitored with a vector-network analyzer with an impedance option (E5061b-005; Keysight) and acquired in real time using a custom MATLAB program. The sensor's dynamic mechanical response, here, the frequency response, was obtained via electromechanical coupling effects using electrical impedance analysis, which provides the electrical impedance magnitude (|Z|) and phase angle (ϕ) spectra of the piezoelectric layer (|Z| and ϕ vs. frequency (f), respectively). Electrical impedance analysis was performed using a stimulus amplitude of 100 mV AC and zero DC bias across a frequency range $f_n \pm 10$ kHz. Sensor signals (f_n) ϕ_n , and Z_n) were acquired using a custom MATLAB program and subsequently used for actuator (UV lamp) control through a data acquisition module (NI USB XSERIES). A fuzzy logic controller was designed using Fuzzy Logic Toolbox in MATLAB R2018b.

2.5. Real-Time Monitoring of Gelation Processes Using Cantilever Sensors. The resonant frequency, phase angle at resonance, and impedance at resonance in air $(f_{n,air}, \phi_{air})$ and Z_{air} respectively) were determined as described in Section 2.4. Experiments began by fabricating a sensor-embedded open cast for the closed-loop controlled curing process. The sensor-embedded cast was fabricated by 3D-printing a hollow cylindrical mold (12 mm in internal diameter and 7 mm in height) using Pluronic F-127 hydrogel around a vertically positioned PEMC sensor using a 20-gauge tapered tip at an extrusion pressure of 9–10 psi and printing speed of 4 mm/s. Pluronic F127 hydrogel was utilized as the mold material for ease of recovery of the cured material. PEGDMA and NIPAm hydrogel precursor solutions (800 µL) were then pipetted into the sensorembedded open cast until the PEMC sensor was completely submerged. The hydrogel was then photocured by exposing the precursor solution to UV light (365 nm; 1200 μ W/cm² at 2 in.; UVGL-58) with open- or closed-loop control. The light source remained at a fixed distance throughout the process (1 cm from the top of the hydrogel surface). 3D printing was done using a previously described custom microextrusion 3D printing process.

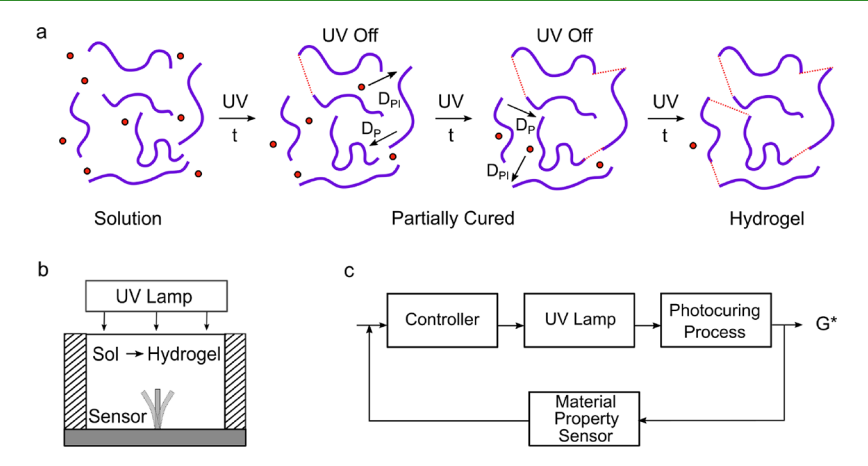


Figure 1. (a) Illustration of the pulsed crosslinking process associated with the closed-loop controlled photopolymerization process. The closed-loop controlled photopolymerization process provides continuous monitoring and control of the extent of photopolymerization reaction and hydrogel mechanical properties via closed-loop controlled UV exposure that involves both UV lamp on- and off-states (D_{PI} and D_{P} represent the diffusivity of the photoinitiator and polymer during the UV lamp off-states). (b) Schematic of the sensor-integrated photopolymerization process (distance between the light source and top of the hydrogel was 1 cm). (c) Block flow diagram for the closed-loop controlled photopolymerization process for programming and quality assurance of hydrogel mechanical properties (complex modulus G^*) highlighting the process (photopolymerization reaction), actuator (UV lamp), sensor (cantilever sensor), and generic controller.

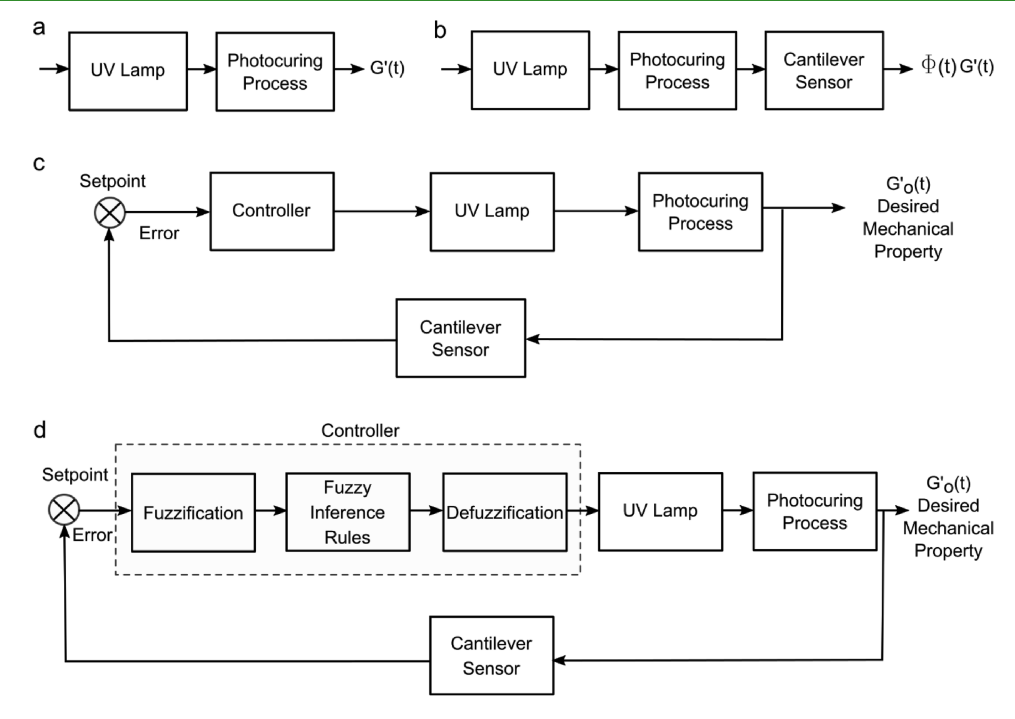


Figure 2. (a) Traditional open-loop photocuring (e.g., photopolymerization) process. (b) Open-loop photopolymerization process with integrated real-time monitoring of hydrogel rheological properties (e.g., storage modulus G') via cantilever sensor phase angle signal. (c) Block flow diagram for a closed-loop controlled photopolymerization process with feedback control based on real-time material property sensing via piezoelectric cantilever sensors (the setpoint is introduced to the error detector—arrow not shown). (d) Plant and controller block diagram for the closed-loop controlled photopolymerization process using fuzzy logic control (the setpoint is introduced to the error detector—arrow not shown).

2.6. Characterization of Hydrogel Low-Frequency Viscoelastic Moduli via Dynamic Mechanical Analysis. Characterization of hydrogel low-frequency viscoelastic properties was done using a dynamic mechanical analyzer (Q800; TA Instruments). Cylindrical test specimens of different concentrations of PEGDMA and PNIPAm hydrogels (diameter, 10.7 ± 0.5 mm; thickness, 4.7 ± 0.5 mm) were photocured as described in the previous section. All measurements were acquired at 25 °C by application of a 15 μ m periodic displacement at a constant frequency (1 Hz) and 5 mN preload force in the compression mode.

2.7. Characterization of Hydrogel Crosslinking via Raman Spectroscopy. Raman spectra of the material at various points

throughout the photopolymerization process were obtained using PeekSeeker (Agiltron Inc.). For the open-loop (i.e., continuous exposure) studies, spectral measurements (n=7) associated with PEGDMA (12 wt %) and NIPAm (10 wt %) hydrogel precursor solutions (2 mL) were recorded in glass scintillation vials (4 mL). Seven glass scintillation vials were filled with 2 mL of PEGDMA and NIPAm precursor solution. The first time point corresponds to unexposed hydrogel precursor solution. Throughout the study, a sample was removed from under the UV light source every minute during continuous exposure and subsequently characterized. For the closed-loop (i.e., pulsed exposure) studies, three samples were placed simultaneously under the light source. One sample was instrumented

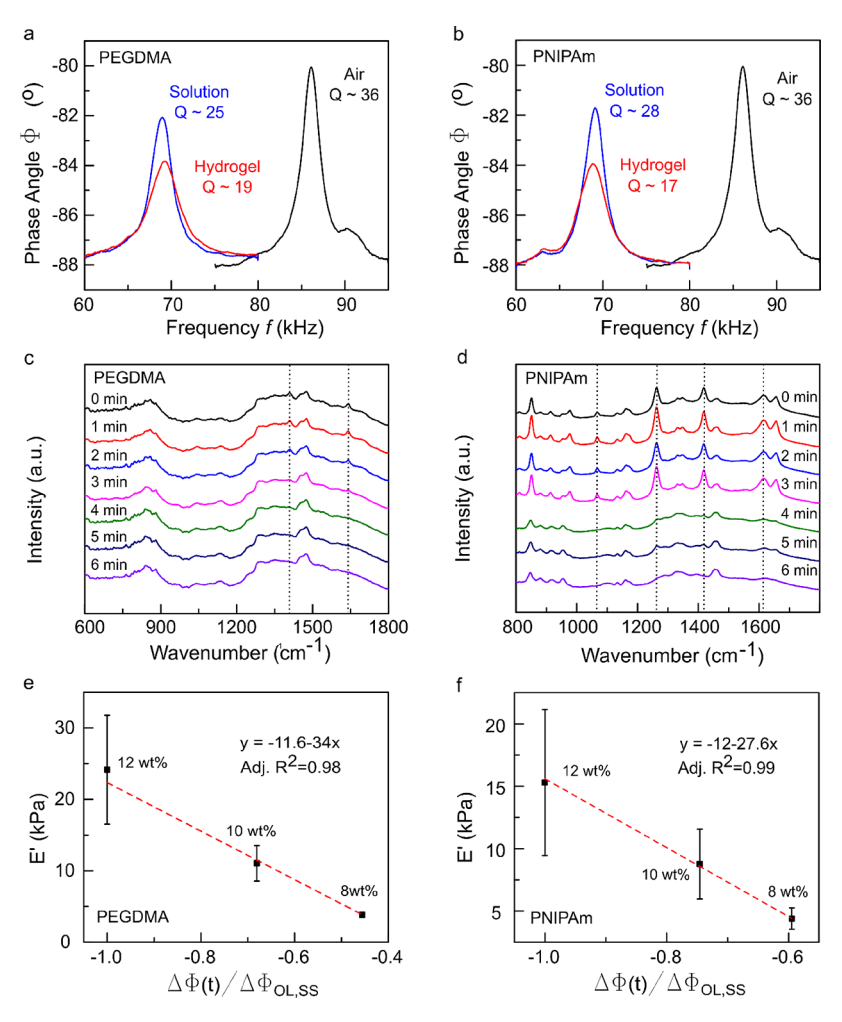


Figure 3. (a) Cantilever frequency response shown as a phase angle spectrum of the PEMC sensor over the frequency range of 60-95 kHz for PEGDMA showing a clear difference in solution and gel phase. (b) Similar frequency response in NIPAm with similar difference in sensor response in solution and gel phase. Raman spectra of (c) PEGDMA and (d) PNIPAm after different amounts of continuous UV exposure. Dashed lines identify peaks that were significantly affected by UV radiation. Correlation between the PEMC sensor response and storage modulus measured at 1 Hz by DMA for (e) PEGDMA and (f) PNIPAm (n = 3 repeated studies).

with a sensor and served to monitor and control the process, a second sacrificial sample was characterized by DMA, and a third sacrificial sample was characterized by Raman spectroscopy. Thus, all samples experienced the same temporal profile of UV light exposure. The spectra were normalized using the peaks at 1475 cm⁻¹ for PEGDMA and 1460 cm⁻¹ for PNIPAm (attributed to H–C–H bending). 30–32

2.8. Characterization of the Hydrogel Network Structure via Scanning Electron Microscopy (SEM). The network structure of the swollen hydrogels was characterized using variable-pressure scanning electron microscope systems (SU-5000; SU-66000; Hitachi). Prior to mounting the membranes, each sample was first hydrated in DIW for at least 24 h. Next, the swollen hydrogels were dried by lyophilization. Samples (10 mm × 10 mm × 10 mm) were freeze-dried for 24 h at -105 °C (FreeZone; Labconco FreeZone). Prior to inserting samples into the scanning electron microscope, the samples were attached by conductive adhesive tape to an aluminum specimen holder and sputter-coated with an ~600 Å layer of platinum (Hummer 6.2; Anatech Ltd.).

2.9. Statistical Analysis. Analysis of the statistical significance among differences in hydrogel mechanical properties was performed using a Student's *t*-test with unequal variance (Excel; Microsoft).

3. RESULTS AND DISCUSSION

3.1. Concept of Closed-Loop Controlled Photopolymerization Processes. As shown in Figure 1a, the

properties of photocurable hydrogels change as a function of the extent of the crosslinking reaction. The focus of this work was to establish a closed-loop controlled photopolymerization process capable of controlling the mechanical properties of photocurable hydrogels. As shown in Figure 1b,c, the closed-loop controlled photopolymerization process is based on real-time monitoring of the hydrogel storage modulus using a cantilever sensor in an open casting configuration.

In contrast to traditional hydrogel photopolymerization processes, which are open-loop and produce materials via steady-state photopolymerization reactions (see Figure 2a), hydrogels fabricated using a closed-loop controlled photopolymerization process are crosslinked by light exposure that is influenced by the real-time signal of a chemical or material property (e.g., rheological property) sensor. As illustrated in Figure 2b—d, real-time material property sensing throughout photopolymerization enables both monitoring and control of hydrogel properties. Here, we establish a novel closed-loop controlled photopolymerization process and compare the properties of hydrogels polymerized using the traditional open-loop processes with those formed using various closed-loop controlled processes. We also compare the performance of different controllers that synergize with on—off UV sources

(actuators), specifically a bang-bang controller (Figure 2c) and Fuzzy logic controller (Figure 2d).

3.2. Monitoring of Hydrogel Photopolymerization Processes Using Cantilever Sensors. In our recent studies, we showed that the phase angle change of PEMC sensors enables real-time monitoring of hydrogel viscoelastic moduli and that the storage moduli of various hydrogels correlated with that obtained using DMA.^{33,34} Thus, prior to discussion of the closed-loop controlled photopolymerization process and the properties of associated hydrogels, we first examined the effect of hydrogel crosslinking on the frequency response of a PEMC sensor for two hydrogels, PEGDMA and PNIPAm. PEGDMA was selected given its wide use in tissue engineering applications and widely available structure and material property characterization data. ^{22,31,35} PNIPAm was selected given its use in stimuli-responsive hydrogel systems, such as alginate-PNIPAm. 36-38 As shown in Figure 3a,b, photopolymerization of PEGDMA and PNIPAm hydrogels is associated with a decrease in both the quality factor and phase angle of the second mode of the PEMC sensor ($f_{air} = 86$ ± 0.16 kHz). For example, as shown in Figure 3a, the phase angle and quality factor changed from $\phi = -81.98 \pm 0.15^{\circ}$ and $Q = 25.3 \pm 0.5$, respectively, to $\phi = -83.7 \pm 0.16^{\circ}$ and $Q = -83.7 \pm 0.16^{\circ}$ 19.6 ± 0.9 upon gelation of a 12 wt % PEGDMA solution. Similarly, gelation of a 10 wt % PNIPAm precursor solution caused a change in the phase angle and quality factor from $\phi =$ $-81.97 \pm 0.36^{\circ}$ and $Q = 26.1 \pm 2.2$ to $\phi = -83.69 \pm 0.25^{\circ}$ and $Q = 19.9 \pm 2.4$ (see Figure 3b). Figure 3a,b shows that material photopolymerization (crosslinking) is associated with a significant change in the phase angle and quality factor of the resonant mode. The second mode was selected based on its use in previous studies for rheological sensing applications. 33,34,39

As shown in Figure 3c,d, we next validated that the change in sensor response (phase angle and quality shift) associated with the exposure of the material to UV was driven by crosslinking within the material. The Raman spectra associated with the PEGDMA and PNIPAm precursor solutions after various exposure times are shown in Figure 3c,d, respectively. The temporal change in the peaks at 1409 and 1642 cm⁻¹ for PEGDMA (Figure 3c) and 1418 and 1612 cm⁻¹ for PNIPAm (Figure 3d), which are associated with C=C bonds, decreased in intensity with increasing UV exposure time and became indistinguishable from baseline values after 6 min. We found that PEGDMA hydrogels exhibited 83 ± 3% conversion based on the peaks at 1409 and 1642 cm⁻¹. PNIPAm hydrogels exhibited 99 and 89% conversion based on the peaks at 1418 and 1612 cm⁻¹, respectively. These studies establish the timescale of the gelation process using an analytical technique and validate that UV exposure under the given experimental setup establishes changes in the material composition associated with photopolymerization reactions that lead to the consumption of reactant C=C bonds.

Having established that photopolymerization of PEGDMA and PNIPAm hydrogels is associated with a large shift in the amplitude (i.e., phase angle) and quality factor of the second mode as well as established the exposure time associated with fully cured hydrogels, we next examined the dependency of the sensor response on the mechanical properties of the surrounding hydrogel. Given that our previous studies have established a positive correlation between the phase angle and quality factor, 33,34 we next characterized the change in sensor phase angle associated with the crosslinking process and

storage modulus of the formed resultant PEGDMA and PNIPAm hydrogels using DMA across the 8-12 wt % range. As shown in Figure 3e,f, a linear relationship was found between the sensor phase angle shift and the storage modulus of the resultant hydrogel (E') formed after the open-loop photopolymerization process. Thus, the data in Figure 3e,f suggest that PEMC sensors may provide the ability to control photopolymerization processes and the mechanical properties of resultant hydrogels through real-time monitoring of the PEMC sensor phase angle.

3.3. Closed-Loop Controlled Hydrogel Photopolymerization Using Bang-Bang Control. The hydrogel photopolymerization process is governed by photopolymerization reactions. Modeling of photopolymerization reactions that drive hydrogel photopolymerization, such as commonly utilized free-radical polymerization reactions, often requires modeling of mass transfer-limited initiation, propagation, and termination reactions. For example, mass transfer limitations are important considerations for polymerization reactions that exhibit large volumes or slow rates.

Given that hydrogel photopolymerization processes exhibit complex dynamics (e.g., systems of rate expressions for reacting molecular species), the polymerization rate has been previously approximated as:

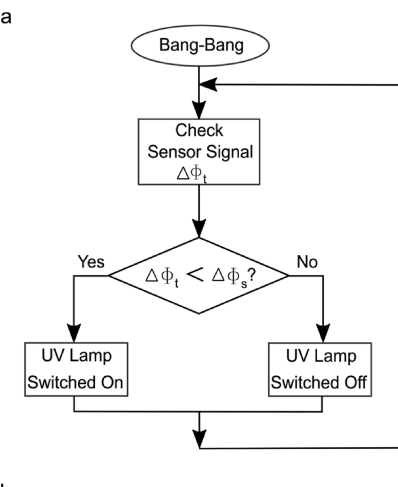
$$R_{\rm p} = k_{\rm p} k_{\rm t}^{0.5} [{\rm M}] \{ \phi I_0 (1 - e^{-\epsilon [{\rm In}]b}) \}^{0.5}$$
 (1)

where R_p is the rate of polymerization, [M] is the concentration of functional groups, k_p and k_t are the propagation and termination rate coefficients, respectively, ϕ is the quantum yield for initiation, I_0 is the incident light intensity, ϵ is the extinction coefficient, [In] is the photoinitiator concentration, and b is the layer thickness. 40 However, given that the dependency of mechanical property on the extent of reaction is dependent on the type of crosslinking chemistry and the molecular weight of reactants, it is challenging to establish a dynamic model that describes the temporal evolution of mechanical property change in terms of the extent of reaction or crosslinking. Thus, we next examined the ability to control the hydrogel photopolymerization process via real-time sensing of the hydrogel storage modulus. The premise of the control system design is based on the ability to sense changes in hydrogel storage modulus (E') via sensor phase angle (ϕ) change (see Figure 3e,f).

The control system design is influenced and constrained by various factors including the process dynamics, production objectives, and available computing power for implementation of the controller. In addition, the types of sensors utilized for process monitoring and actuators utilized for modulating process inputs have a major effect on control system design. While various types of actuators exist, such as proportional actuators, the UV sources (lamps) utilized for photopolymerization processes are typically on-off actuators. In other words, the lamp is either in an off-state, which provides no UV exposure to the material, or on-state, which provides UV exposure at a constant intensity.

Bang-bang control has been widely utilized to control a range of physical and chemical processes using on-off actuators. ⁴¹⁻⁴⁴ Thus, we first created a closed-loop controlled photopolymerization process with bang-bang control and examined the in situ crosslinking and final properties of the hydrogel. Given that the mechanical properties of a hydrogel serve as quality indicators in various applications, particularly

tissue engineering, drug discovery, and energetics, the bangbang controller was designed to control the modulus of the resultant hydrogel based on a logic condition. The plant and controller block diagram for the bang-bang controller is provided in Figure 4a. Given that the sensor phase angle is



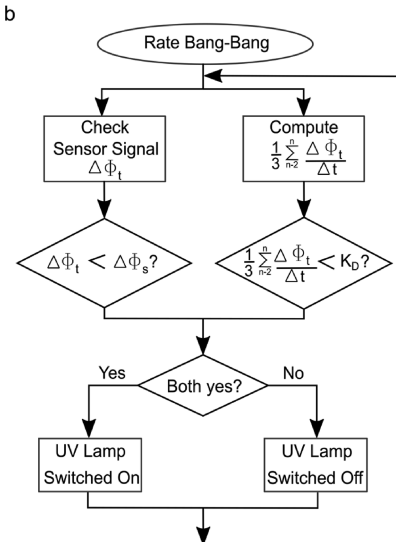


Figure 4. Flow chart for (a) the bang-bang and (b) rate-based bangbang controllers for the closed-loop controlled hydrogel photopolymerization process.

related to the modulus of the material (see Figure 3e,f), the setpoint of the UV lamp output (i.e., the condition that the lamp's output is in the on- or off-state) was defined in terms of a threshold in phase angle change as:

If
$$\Delta \phi < \Delta \phi_s$$
, then actuator (UV lamp) on;

where $\Delta\phi_{\rm s}$ is the user-defined setpoint in the material mechanical property (E') through the relationships shown in Figure 3e,f and is defined in reference to the total phase angle change associated with the open-loop steady-state curing process $(\Delta \phi_{\rm OL})$. Given that the resonant frequency response of the sensor is associated with an added mass effect, 45,46 the sensor resonant frequency response was used to trigger the controller immediately following filling of the cast with precursor material. To reduce computing demands during the initial sensor stabilization periods of the study, the

photopolymerization process was initiated by the controller turning on the UV lamp after 3 min of achieving a stable sensor baseline signal.

In addition to a classic bang-bang controller, we also created and examined the performance of a modified bang-bang controller that also considered the rate of change in sensor response in the control decision, which we refer to as a ratebased bang-bang controller. The flow chart of the rate-based bang-bang controller is shown in Figure 4b. While the classic bang-bang controller (see eq 2) is designed to control only the modulus of the cured material, the rate-based bang-bang controller is designed to control both the crosslinking rate and the modulus. In contrast to the bang-bang controller, which utilized the instantaneous value of the sensor phase angle (i.e., the material's storage modulus), the rate-based bang-bang controller controlled the UV lamp output based on a moving average (three-point) of the time rate of change in the sensor phase angle (material storage modulus) as:

If
$$\Delta \phi < \Delta \phi_{\rm s}$$
 and $\frac{1}{3} \sum_{n-2}^{n} \left(\frac{\phi_{t} - \phi_{t-1}}{\Delta t} \right)$
 $< K_{\rm D}$, then actuator on;
Else, actuator off. (3)

where $n \ge 3$ and K_D is a user-defined controller parameter that exhibits units of °/s.

A comparison of the bang-bang controlled, rate-based bangbang controlled, and open-loop photopolymerization processes in terms of the temporal curing profile (sensor data) is provided in Figure 5a-d. A comparison of bang-bang controlled photopolymerization of PEGDMA and PNIPAm $(\Delta \phi_s = 0.54 \Delta \phi_{OL})$ and $\Delta \phi_s = 0.57 \Delta \phi_{OL}$, respectively) with the traditional open-loop photopolymerization process in which the UV lamp remains continuously in the on-state is shown in Figure 5a,b. The state of the actuator is indicated as green (on) or red (off) circles. As shown in Figure 5a,b, the controller effectively stopped the photopolymerization process of both hydrogels near their setpoint of $0.55\Delta\phi_{\rm OL}$. The bang-bang controller resulted in continuous UV exposure until the setpoint was reached. A delay of ~90 s in the phase angle change following the onset of UV exposure was observed in both PEGDMA and PNIPAm. The cure times for the bangbang controller (i.e., the time required to reach the setpoint) were 3.0 \pm 0.1 and 2.9 \pm 0.8 min for PEGDMA and PNIPAm, respectively. After this period, the bang-bang controller maintained the UV lamp predominantly in the off-state with the exception of nine triggering events (~2 s UV exposure/ event) in PEGDMA following the steady state. As shown in Figure 5a,b, the bang-bang controller resulted in a small overshoot in the setpoint for both the PEGDMA and PNIPAm systems. For example, the PEGDMA and PNIPAm systems exhibited 11 and 19% overshooting. Overshooting was attributed to the continued crosslinking reactions from the activated photoinitiator for a brief period after stopping UV exposure.

Given the bang-bang controller resulted in overshooting, we next examined if the incorporation of rate control into the classical bang-bang controller could potentially reduce the extent of overshooting. The performance of a rate-based bangbang controller with various tuning parameters and the bangbang controller is shown in Figure 5c,d. The rate-based controller data shown in Figure 5c,d correspond to $2K_D$ =

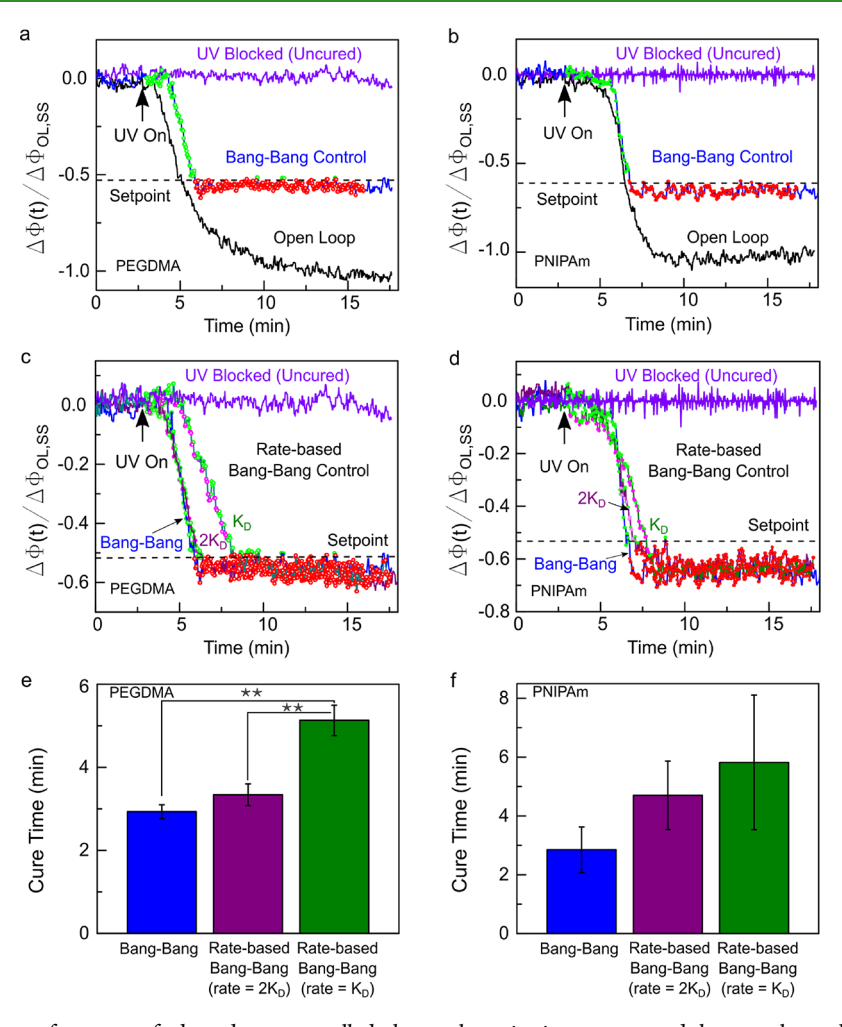


Figure 5. Comparison of the performance of a bang-bang controlled photopolymerization process and the open-loop photopolymerization process for (a) PEGDMA and (b) PNIPAm in terms of the sensor phase angle response (i.e., material storage modulus response). The dotted line represents the setpoint for the material final storage modulus in terms of the sensor phase angle. Green circles represent UV lamp on, magenta circles represent UV lamp off due to the rate being faster than the desired rate, and red circles represent lamp off due to reaching the desired crosslinking setpoint. Sensor data associated with repeated studies in which the UV source was blocked served as a negative control. Comparison of the performance of the bang-bang and rate-based bang-bang controlled photopolymerization processes with the open-loop photopolymerization process for (c) PEGDMA and (d) PNIPAm in terms of the sensor phase angle response (i.e., material storage modulus response). Comparison of cure times obtained for each of the controllers for (e) PEGDMA and (f) PNIPAm. Experiments were done in triplicate (*p < 0.05; **p < 0.01).

-0.008 and $K_{\rm D}$ = -0.004 °/s (negative sign represents decreasing phase angle with increasing storage modulus). K_D was selected from the three-point moving average of the time rate of change in the phase angle in the linear response region from 5 to 7 min for the bang-bang controller, which is related to the time rate of change in the storage modulus (see Figure 3e,f). Subsequently, $2K_D$ was then selected such that at a maximum, 25% of the data points from the three-point moving average of the time rate change in phase angle would be greater than the selected value. Hence, the tuning parameter $K_{\rm D}$ provided an upper threshold for the rate of the photopolymerization reaction. The setpoints used for the degree of crosslinking were $0.54\Delta\phi_{\mathrm{OL}}$ and $0.57\Delta\phi_{\mathrm{OL}}$ of the total cure in the open loop for PEGDMA and PNIPAm, respectively. As shown in Figure 5c,d, incorporation of the rate condition in the bang-bang controller (i.e., the rate-based bang-bang controller) enabled the system to slow the cure rate and resulted in UV lamp switching throughout the continuous curing period associated with the bang-bang controller. The effect of the magnitude of the tuning parameter is also evident. For example, as shown in Figure 5c, the rate-based controller

resembles the curing profile of the bang-bang controller for the selected tuning parameter $2K_D = -0.008$ °/s.

Given that the controllers exhibited significant differences in the temporal curing profile as measured through sensor phase angle change (i.e., material storage modulus change), we next examined the cure times for each controller and final mechanical properties of the hydrogels formed. The cure time associated with each controller is presented in Figure 5e,f. The bang-bang controller and the rate-based bang-bang controllers exhibited average cure times of 2.9, 3.3 $(2K_D)$, and 5.1 (K_D) min for PEGDMA, respectively. The bang-bang controller and the rate-based bang-bang controllers exhibited average cure times of 2.8, 4.7 $(2K_D)$, and 5.8 (K_D) minutes for PNIPAm, respectively. While the differences among cure times for the bang-bang and both rate-based bang-bang controllers were examined (p = 0.002; n = 3 repeated samples) for the PEGDMA system, the differences in cure time among the different controllers for the PNIPAm system were not statistically significant. The bang-bang controller resulted in the most rapid cure time for PEGDMA hydrogels.

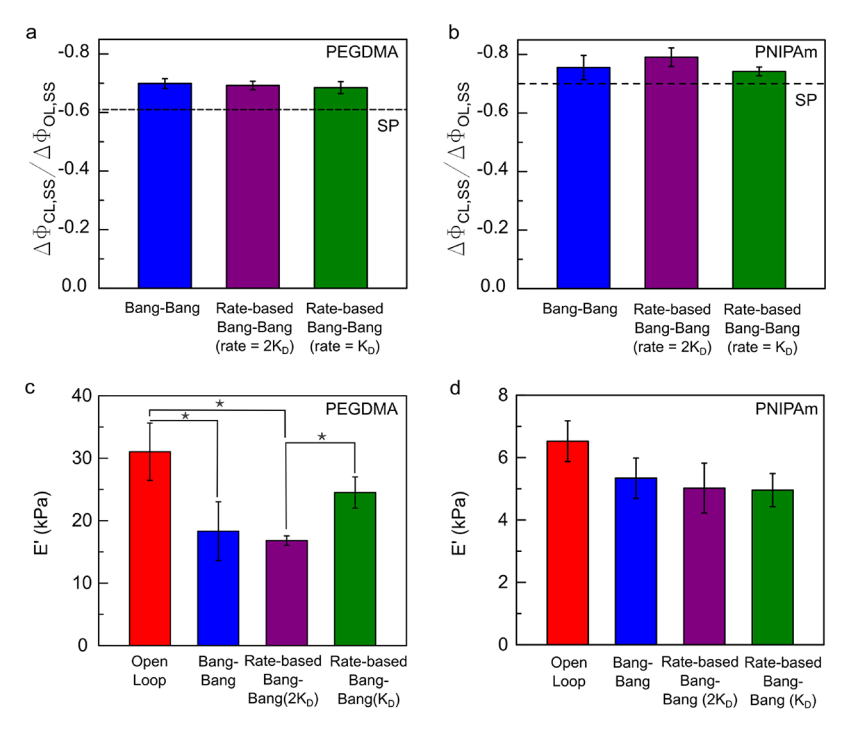


Figure 6. Comparison of controller performance for closed-loop controlled photopolymerization in terms of the steady-state sensor phase angle shifts corresponding to the sensor time series data shown in Figure 5 for (a) PEGDMA and (b) PNIPAm. Comparison of controller performance for closed-loop controlled photopolymerization in terms of the storage modulus of the resultant hydrogel obtained by DMA corresponding to the sensor time series data shown in Figure 5 for (c) PEGDMA and (d) PNIPAm (*p < 0.05).

As previously discussed, as a motivation for incorporating a rate constraint into the classical bang-bang controller in terms of the tuning parameter K_D , overshooting was observed (Figure 5a-d) and attributed to the continued crosslinking reactions associated with the unreacted activated photoinitiator. A comparison of the extent of overshooting observed among the different controllers for the PEGDMA and PNIPAm hydrogels is shown in Figure 6a,b. The overshooting values for PEGDMA were 7, 10 $(2K_D)$, and 11% (K_D) for the bang-bang and rate-based bang-bang controllers, respectively (n = 3 samples). The overshooting values for PNIPAm were 19, 14 $(2K_D)$, and 11% (K_D) for the bang-bang and rate-based bang-bang controllers, respectively (n = 3 samples). The differences among the means were not statistically significant for the sample size examined, suggesting that all controllers led to an irreversible overshoot in the storage modulus of the cured hydrogels. However, most importantly, the controllers enable the fabrication of PEGDMA and PNIPAm hydrogels within ~7 and 19% of the anticipated material property based on the sensor data response.

Having established the performance of the bang-bang controlled photopolymerization processes in terms of the dynamic sensor response (i.e., sensor phase angle time-series data), we next examined if the variation in the temporal profile of UV exposure affected the mechanical properties of the cured hydrogels. To demonstrate the ability to achieve various setpoints in the cured hydrogel's storage modulus, different setpoints of $0.60\Delta\phi_{\rm OL}$ and $0.70\Delta\phi_{\rm OL}$ were utilized for PEGDMA and PNIPAm, respectively. Figure 6a–d shows the performance of the bang-bang and rate-based bang-bang controllers for PEGDMA and PNIPAm hydrogels in terms of the resultant sensor response and storage modulus obtained by DMA. As shown in Figure 6a,b, all controllers resulted in overshooting of the setpoint in terms of the percentage of

open-loop sensor shift $(\Delta\phi_{\rm OL})$, which ranged from 14 to 16% and 5 to 15% among the controllers for PEGDMA and PNIPAm, respectively. However, differences in overshoot among the controllers as characterized by sensor data were not statistically significant. While sensor phase angle data correlate with the hydrogel storage modulus for various material systems³⁴ (also see Figure 3e,f), it provides an indirect measure of the low-frequency storage modulus, which is utilized as a performance metric across various applications. As shown in Figure 6a, the bang-bang and rate-based bangbang controllers with the lowest tuning parameter value resulted in the least amount of overshoot for the PEGDMA system. Interestingly, while differences among the sample properties were not significant based on the final sensor signal, the controllers resulted in PEGDMA hydrogels that exhibited statistically significant differences in low-frequency storage modulus obtained from DMA (open-loop = 31 ± 4.6 kPa, bang-bang = 18.3 \pm 4.7 kPa, rate-based bang-bang (2 K_D) = 16.8 \pm 0.7 kPa, and rate-based bang-bang (K_D) = 24.5 \pm 2.5 kPa; n = 3 samples per controller). As shown in Figure 6c, the difference in storage modulus of PEGDMA hydrogels cured using the two different tuning parameters for the rate-based bang-bang controller was statistically significant (p = 0.036, 95% confidence interval).

As shown in Figure 6d, while the storage modulus varied among the hydrogels produced using the different controllers (open-loop = 6.5 ± 0.6 kPa, bang-bang = 5.3 ± 0.6 kPa, rate-based bang-bang ($2K_{\rm D}$) = 5.0 ± 0.8 kPa, rate-based bang-bang ($K_{\rm D}$) = 4.9 ± 0.5 kPa; n=3 samples per controller), the differences among the controller performance for PNIPAm hydrogels based on the storage modulus obtained by DMA were also insignificant, similar to the differences among the final sensor signals (see Figure 6b). Thus, our results show that the rate of crosslinking and temporal profile of UV exposure

can affect the resultant low-frequency storage modulus of the PEGDMA hydrogel, but this sensitivity to the crosslinking rate was not observed in the PNIPAm system for the rates examined.

Similar to the studies done with different final property setpoints (see Figure 5), we examined the cure time associated with the different controllers for the setpoints of $0.60\Delta\phi_{\rm OL}$ and $0.70\Delta\phi_{\rm OL}$ utilized for PEGDMA and PNIPAm, respectively. Similar to the trends among cure times for the different controllers for the setpoints of 0.54 $\Delta\phi_{\rm OL}$ (PEGDMA) and $0.57\Delta\phi_{\rm OL}$ (PNIPAm), the bang-bang controller and the ratebased bang-bang controller with the lowest tuning parameter exhibited statistically significant differences in cure time for the PEGDMA hydrogels but not the PNIPAm hydrogels. The average crosslinking rate as defined in terms of the rate of change in sensor response throughout the first few minutes of the photopolymerization processes among the controllers ranged from -0.00316 ± 0.0007 to -0.0057 ± 0.002 °/s and was utilized in controller parameter (K_D) tuning.

Differences in the closed-loop controlled photopolymerization processes between the two hydrogel systems (PEGDMA vs. PNIPAm) could be attributed to various factors, such as differences among the molecular weights and compositions of reactive species as well as the crosslinking mechanism. For example, NIPAm is a monomer and requires a crosslinker to undergo a free-radical polymerization reaction, while PEGD-MA photopolymerization does not require the addition of a crosslinker. It has been previously found that the heterogeneity in the polymer networks increases with the increase in crosslinker-to-monomer ratio in the precursor solution⁴⁷ and crosslinker reactivity. 48 The magnitude of the hydrogel storage modulus exhibited a correlation with the total UV exposure time for PEGDMA hydrogels. In the case of bulk open-loop photopolymerization of pure PEGDMA, the network consists of a homologous repetition of PEGDMA monomers that have a long kinetic chain length.⁴⁹ Thus, the difference in the storage modulus of PEGDMA hydrogels processed by bangbang and rate-based bang-bang controlled photopolymerization (K_D) could be attributed to differences among network structures due to the extended diffusive timescale for unreacted monomers and oligomers in the rate-based bang-bang controlled photopolymerization process relative to the bangbang controlled photopolymerization process. For example, the UV lamp remains in an off-state for longer periods during ratebased bang-bang controlled photopolymerization vs. bangbang control. It is also useful to consider the diffusive length scale associated with an unreacted precursor species associated with the time in which the UV lamp remains in an off-state during the photopolymerization process as the reactive species could potentially adopt a position and configuration in the resultant hydrogel network that differs from that achieved in the case of continuous UV exposure. While the diffusion constant changes throughout the photopolymerization reaction, the diffusion coefficient of a PEGDMA precursor in a hydrogel ($D = 10^{-9} \text{ cm}^2/\text{s}$)⁵⁰ provides a conservative estimate for estimating the length over which an unincorporated molecular species could diffuse through the network during the UV lamp off-state. Given that the duration of the UV lamp off-state (t) was, at greatest, 15 s (see Figure 5a-d), an unreacted macromolecular species may diffuse at $L = (tD)^{0.5} \approx$ 2.3 μ m, which is greater than the mesh size of PEGDMA hydrogels (4-35 nm),⁵¹ which suggests that diffusion processes during photopolymerization processes may be

controlled and facilitate the formation of alternative network structures than obtained from diffusion-limited polymerization reactions. Fang et al. investigated the diffusion-limited photopolymerization in scanning microstereolithography. S They found that pulsed laser curing created a diffusiondominant effect that increases the achievable feature resolution relative to that achieved by continuous wave polymerization. S These considerations and calculations combined with the observation of statistically significant differences between the storage moduli of PEGDMA hydrogels cured using the bangbang controllers suggest that the hydrogels formed by the bang-bang and rate-based bang-bang controllers (K_D) exhibit differences in the network structure. It has been previously noted that due to the random nature of radical propagation in chemically crosslinked polymerization, hydrogels produced by such a method result in a relatively more heterogeneous network structure as the number of arms per crosslinking point is not static.⁵³

To directly characterize the differences in network structure among the hydrogels formed by the various controllers, images of the hydrogel network structure were obtained using scanning electron microscopy (SEM). The results of this analysis are shown in Figure 7. Specifically, SEM images of

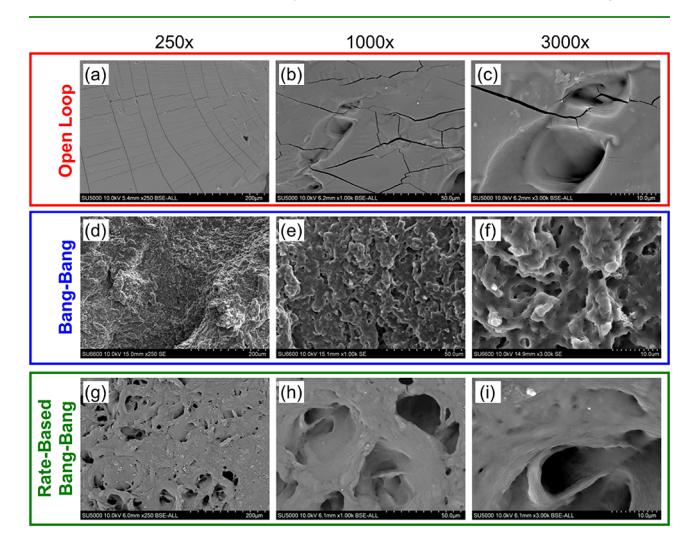
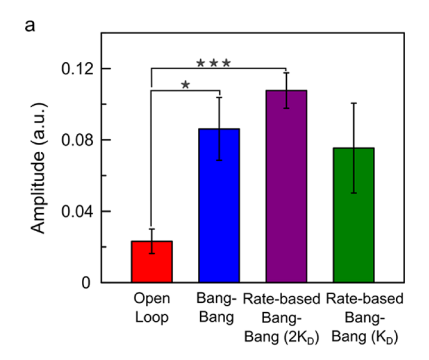


Figure 7. Scanning electron microscopy (SEM) images of PEGDMA hydrogels prepared via open-loop (a-c, red outline), bang-bang (d-f, blue outline), and rate-based bang-bang (rate = K_D ; g-i, green outline) controlled photopolymerization. The magnification within a column is the same and increases from 250× to 3000× (left to right).

PEGDMA hydrogels fabricated using open-loop (outlined in red), bang-bang (outlined in blue), and rate-based bang-bang control (outlined in green) are shown in Figure 7a-c, Figure 7d-f, and Figure 7g-i, respectively. Note that the microscope magnification is the same within a column and increases from 250× to 3000× as you move left to right within a row. As posited above, the SEM images shown in Figure 7 highlight how the three controllers (i.e., temporal profiles to UV exposure) result in three drastically different network structures of the swollen hydrogels. First, focusing our attention on the SEM images for PEGDMA hydrogels fabricated via open-loop photocuring (i.e., continuous exposure), we observe little evidence of microscopic pore formation across the hydrogel (Figure 7a). The sparse number of pores in the higher-magnification images (Figure 7b,c) is approximately 10 μ m in diameter, although it is not clear



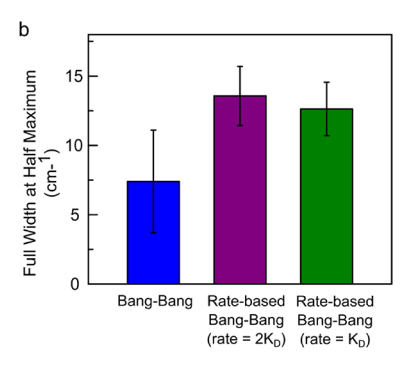


Figure 8. (a) Amplitude of the peak at 1409 cm⁻¹ in the Raman spectra of PEGDMA hydrogels cured using the various closed-loop controlled photopolymerization processes. (b) Characterization of controller performance in terms of the full width at half maximum of the peak at 1409 cm⁻¹ in the Raman spectra (*p < 0.05; ***p < 0.001).

whether this pore network is fully percolated over the entire thickness of the hydrogel. In contrast, as seen in the SEM images in Figure 7d-i, a highly porous, percolated network structure is observed for PEGDMA hydrogels fabricated by both the bang-bang and rate-base bang-bang controlled photopolymerization processes. Additionally, we observed that the pore structure varied between hydrogels fabricated by two different bang-bang controllers. Overall, the pores appear to be much smaller for hydrogels fabricated using bangbang control than compared with the rate-based bang-bang counterparts (Figure 7f vs Figure 7i). The SEM images shown in Figure 7 underscore the above assertion that diffusion processes during pulsed photopolymerization processes may be directly controlled through the choice of controller and enable the formation of alternative network structures than obtained from polymerization processes based on continuous exposure to high-intensity UV light. To further evaluate the differences in the hydrogel network structure, we next characterized the hydrogels formed using the various controllers using Raman spectroscopy.

Raman spectroscopy has been utilized for the compositional analysis of hydrogels. ³¹ In addition, the Raman spectra of hydrogels have also been utilized to characterize the structure of hydrogels. 54,55 For example, the sharpness of peaks in the Raman spectra as characterized by the full width at half maximum (FWHM) has been associated with the extent of network structure heterogeneity. As shown in Figure 8a, we found that the amplitude of the peak at 1409 cm⁻¹ associated with C=C bonds differed among the various controllers, suggesting that more C=C bonds were consumed from the rate-based bang-bang controlled photopolymerization process $(K_{\rm D})$, which exhibited the lowest curing rate among the closedloop controlled processes. As shown in Figure 8b, we examined FWHM for the peak at 1409 cm⁻¹. The FWHM was the smallest for the bang-bang controlled photopolymerization process $(7.4 \pm 3.7 \text{ cm}^{-1})$ and increased for the rate-based bang-bang controllers $(2K_{\rm D} = 13.5 \pm 2.1 \text{ cm}^{-1}; K_{\rm D} = 12.6 \pm 10.0 \text{ c$ 1.9 cm⁻¹). While the differences in FWHM were not statistically significant at a 95% confidence level, the p-value associated with the difference among the means of the FWHM for the bang-bang controller vs. the rate-based bang-bang controller was p = 0.08, which suggests that the materials may exhibit meaningful differences in material structure. These data suggest that the FWHM increased as the cure rate decreased, indicating that decreasing the cure rate of PEGDMA hydrogels is associated with an increase in network heterogeneity. We note that changes in curing process parameters have resulted in

materials that exhibit differences in some properties, such as the Young's modulus, while not impacting other properties, such as the strength.

3.4. Closed-Loop Controlled Hydrogel Photopolymerization Using Fuzzy Logic Control. The results presented in Figures 3-8 demonstrate that one can utilize bang-bang controlled photopolymerization processes to control the composition, structure, and properties of hydrogels during fabrication as well as reproducibly fabricate hydrogels of a predetermined storage modulus. However, while the bangbang controllers did provide control over the hydrogel storage modulus during crosslinking, the various bang-bang controllers examined exhibited overshoot. Thus, we next examined if the overshooting associated with the closed-loop controlled photopolymerization process could be mitigated through the use of an alternative control system. Thus, we next evaluated the use of fuzzy logic to control the photopolymerization process instead of bang-bang feedback control. Fuzzy logic provides with a rule-based control approach based on linguistic expressions⁵⁶ and has been a useful control system for processes that exhibit complex dynamics,⁵⁷ such as mass transfer-limited photopolymerization reactions. Given that the bang-bang controllers enabled fabrication of PEGDMA that exhibited statistically significant differences in structure and properties (see Figures 6-8), the fuzzy logic controller was validated using PEGDMA (12 wt %).

The fuzzy logic controlled photopolymerization process was implemented as follows. Two inputs were defined: the relative phase angle shift and the three-point moving average of time rate change in the phase angle. Each input was normalized within a range of [-1, 1]. Input 1 had three membership functions, namely, far, close, and closest, which describe the distance from the degree of crosslinking setpoint. Input 2 had four membership functions, namely, slowest, slow, fast, and fastest, which describe the crosslinking rate as defined by the three-point moving average of time rate change in sensor phase angle. Both the inputs were defined as triangular functions. The output that was defined as a Gaussian function had three membership functions, namely, short, long, and longest, which describe the amount of time the UV lamp would be switched off. Tuning of each membership function associated with the inputs and the rules of the controller were defined in such a way that as Input 1 got closer to the modulus setpoint or Input 2 increased too fast, the output value will increase, hence increasing the amount of time the UV lamp would stay in the off-state. Outputs were changed to check the applicability of the controller and its effectiveness in controlling the crosslinking rate of photopolymerization (gelation) reaction. For example, consider two potential output ranges that could be selected for the fuzzy logic controller, [0,15] or [0,7] s. The controller action associated with the relatively larger output range (e.g., [0.15]) will penalize the plant more for increasing too rapidly or approaching the modulus setpoint. The extent of this penalty would be reduced by selecting the relatively lower output range. Various combinations of Input 1 and Input 2 were used to define rules for the output. In total, 12 rules were defined by which the output was decided in each cycle. The rules associated with the fuzzy logic controlled photopolymerization process are:

If (Input 1 is far) and (Input 2 is slowest)

```
, then (output is short);
If (Input 1 is far) and (Input 2 is slow)
  , then (output is short);
If (Input 1 is far) and (Input 2 is fast)
  , then (output is longest);
If (Input 1 is far) and (Input 2 is fastest)
  , then (output is longest);
If (Input 1 is close) and (Input 2 is slowest)
  , then (output is long);
If (Input 1 is close) and (Input 2 is slow)
  , then (output is long);
If (Input 1 is close) and (Input 2 is fast)
  , then (output is longest);
If (Input 1 is close) and (Input 2 is fastest)
   , then (output is longest);
If (Input 1 is closest) and (Input 2 is slowest)
   , then (output is long);
If (Input 1 is closest) and (Input 2 is slow)
  , then (output is long);
If (Input 1 is closest) and (Input 2 is fast)
  , then (output is longest);
If (Input 1 is closest) and (Input 2 is fastest)
  , then (output is longest).
                                                             (4)
```

The performance of the fuzzy logic controlled photopolymerization process associated with two different sets of membership functions (μ_i) for closed-loop controlled gelation of PEGDMA hydrogels is shown in Figure 9. While overshooting was still observed in PEGDMA hydrogel photopolymerization for some selections of the membership function (e.g., μ_2 as shown in Figure 9; associated with a smaller output range), it was also possible to eliminate overshooting of the setpoint of the sensor phase angle (i.e., hydrogel storage modulus) through alternative selections (e.g., μ_1). For example, we found that it was possible for the fuzzy logic controller to provide minimal crosslinking rates that led to undershooting of the controller setpoint of $0.7\Delta\phi_{\mathrm{OL}}$ within

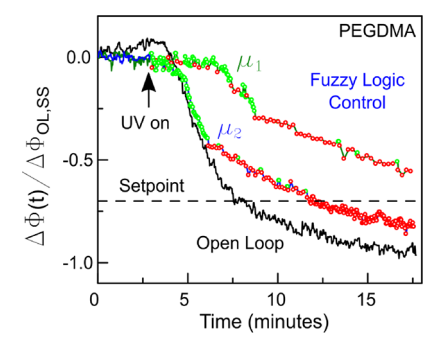


Figure 9. Comparison of the fuzzy logic controller performance for multiple membership functions (μ_i) in terms of the sensor phase angle response with the open-loop photopolymerization process for PEGDMA hydrogels (12 wt %).

the set time period for which the program was ran for (i.e., the total time set at the start of the process). Hence, by adjusting the membership functions of the input, the output, and the crosslinking rate, overshooting of the storage modulus setpoint can be potentially eliminated. This result suggests that fuzzy logic control may also provide a useful approach for closedloop controlled material photopolymerization processes.

Consistent with the observations in this study on photocured materials subjected to discontinuous and irregular pulses of UV light, the temporal profile of UV exposure has also been shown to affect the properties of other photocurable materials. For example, light source switching between on-off states has been shown to provide temporal and spatial control on the photocrosslinking process. 58-60 In reversible addition-fragmentation chain transfer (RAFT) polymerization and ultrasonic-RAFT type of polymerization reactions, it was found that light source switching coincided with starting and termination of monomer conversion. 60,61 The intensity of incident light has also been shown to affect the dispersity of the photocured polymers.⁶⁰ Hence, the integration of monitoring and control principles in hydrogel photopolymerization processes could provide new opportunities for controlling hydrogel mechanical properties under practical processing (e.g., open-cast photopolymerization processes). Further, it may be possible to achieve materials that exhibit novel structure and properties relative to those obtained from traditional open-loop polymerization processes (continuous crosslinking) based on "diffusion-dominant structures" that are achieved through pulsed or discontinuous polymerization processes.

4. CONCLUSIONS

This work provided an advance in the processing of hydrogels. Here, we presented closed-loop controlled hydrogel photopolymerization processes based on real-time monitoring of hydrogel mechanical properties via dynamic-mode cantilever sensors. We found that the closed-loop photopolymerization processes enabled fabrication of hydrogels with a controlled network structure and storage modulus. We also found that the network structure and storage modulus of PEGDMA hydrogels were dependent on the extent and temporal profile of UV light exposure. SEM studies showed that the network structure of PEGDMA hydrogels varied among all controller designs, suggesting that it could be tuned with the appropriate choice of controller and tuning parameters. While bang-bang control exhibited setpoint overshooting for both the PEGDMA and PNIPAm hydrogels, the overshoot was consistent, suggesting

the possibility for overshoot compensation through reduction of the initial setpoint selection. Overshooting the setpoint of the cured hydrogel storage modulus was mitigated by the use of a fuzzy logic controller. Closed-loop controlled photopolymerization processes offer the potential to improve the reproducibility and quality of hydrogels and hydrogel-based products, which remains a critical challenge across various fields that employ hydrogels, including tissue engineering. Controlled (e.g., pulsed) photopolymerization processes may offer the potential to achieve structures and properties in hydrogels that cannot otherwise be realized via polymerization under continuous light exposure.

AUTHOR INFORMATION

Corresponding Author

Blake N. Johnson — Department of Industrial and Systems Engineering, Macromolecules Innovation Institute, and Department of Chemical Engineering, Virginia Tech, Blacksburg, Virginia 24061, United States; Department of Materials Science and Engineering, Virginia Tech, Blacksburg, Virginia 24061, United States; Present Address: 121 Durham Hall, 1145 Perry St., Blacksburg, Virginia 24061, United States (B.N.J.); orcid.org/0000-0003-4668-2011; Email: bnj@vt.edu; Fax: 540-231-3322

Authors

- Manjot Singh Department of Industrial and Systems Engineering, Virginia Tech, Blacksburg, Virginia 24061, United States
- Junru Zhang Department of Industrial and Systems Engineering, Virginia Tech, Blacksburg, Virginia 24061, United States
- **Keturah Bethel** Department of Chemical and Biomolecular Engineering, Clemson University, Clemson, South Carolina 29634, United States
- Yang Liu Macromolecules Innovation Institute, Virginia Tech, Blacksburg, Virginia 24061, United States
- Eric M. Davis Department of Chemical and Biomolecular Engineering, Clemson University, Clemson, South Carolina 29634, United States; © orcid.org/0000-0002-5633-5489
- Haibo Zeng Department of Electrical and Computer Engineering, Virginia Tech, Blacksburg, Virginia 24061, United States
- **Zhenyu Kong** Department of Industrial and Systems Engineering, Virginia Tech, Blacksburg, Virginia 24061, United States

Complete contact information is available at: https://pubs.acs.org/10.1021/acsami.1c11779

Author Contributions

M.S., H.Z., Z.K., and B.N.J. conceived the process and designed the experimental study. M.S. and B.N.J. constructed the process testbed. M.S. performed all experimental studies. J.Z. assisted with closed-loop controlled photopolymerization studies. Y.L. assisted with Raman spectroscopy studies. K.B. performed SEM characterization of the hydrogel samples under the guidance of E.M.D. M.S. and B.N.J. analyzed the data. M.S., H.Z., Z.K., E.M.D., and B.N.J. wrote the manuscript. M.S., J.Z., Y.L., H.Z., Z.K., K.B., E.M.D., and B.N.J. edited the manuscript.

Notes

The authors declare no competing financial interest.

ACKNOWLEDGMENTS

The authors are grateful for the generous support of the National Science Foundation (CMMI-1739318 and CBET-1915787). K.B. also acknowledges the generous support of the Department of Education Graduate Assistance in Areas of National Need (GAANN) Fellowship (award no. P200A180076).

REFERENCES

- (1) Ullah, F.; Othman, M. B. H.; Javed, F.; Ahmad, Z.; Akil, H. M. Classification, processing and application of hydrogels: A review. *Mater. Sci. Eng., C* **2015**, *57*, 414–433.
- (2) Akhtar, M. F.; Hanif, M.; Ranjha, N. M. Methods of synthesis of hydrogels ... A review. *Saudi Pharm. J.* **2016**, 24, 554–559.
- (3) Hoffman, A. S. Hydrogels for biomedical applications. *Adv. Drug Delivery Rev.* **2012**, *64*, 18–23.
- (4) Buenger, D.; Topuz, F.; Groll, J. Hydrogels in sensing applications. *Prog. Polym. Sci.* **2012**, *37*, 1678–1719.
- (5) Anjali, J.; Jose, V. K.; Lee, J.-M. Carbon-based hydrogels: synthesis and their recent energy applications. *J. Mater. Chem. A* **2019**, 7, 15491–15518.
- (6) Hoare, T. R.; Kohane, D. S. Hydrogels in drug delivery: Progress and challenges. *Polymer* **2008**, 49, 1993–2007.
- (7) Lee, K. Y.; Mooney, D. J. Alginate: properties and biomedical applications. *Prog. Polym. Sci.* **2012**, *37*, 106–126.
- (8) Lee, K. Y.; Mooney, D. J. Hydrogels for Tissue Engineering. *Chem. Rev.* **2001**, *101*, 1869–1880.
- (9) Banerjee, A.; Arha, M.; Choudhary, S.; Ashton, R. S.; Bhatia, S. R.; Schaffer, D. V.; Kane, R. S. The influence of hydrogel modulus on the proliferation and differentiation of encapsulated neural stem cells. *Biomaterials* **2009**, *30*, 4695–4699.
- (10) Li, Z.; Guo, X.; Palmer, A. F.; Das, H.; Guan, J. High-efficiency matrix modulus-induced cardiac differentiation of human mesenchymal stem cells inside a thermosensitive hydrogel. *Acta Biomater.* **2012**, *8*, 3586–3595.
- (11) Chatterjee, K.; Lin-Gibson, S.; Wallace, W. E.; Parekh, S. H.; Lee, Y. J.; Cicerone, M. T.; Young, M. F.; Simon, C. G. The effect of 3D hydrogel scaffold modulus on osteoblast differentiation and mineralization revealed by combinatorial screening. *Biomaterials* **2010**, *31*, 5051–5062.
- (12) Parekh, S. H.; Chatterjee, K.; Lin-Gibson, S.; Moore, N. M.; Cicerone, M. T.; Young, M. F.; Simon, C. G. Modulus-driven differentiation of marrow stromal cells in 3D scaffolds that is independent of myosin-based cytoskeletal tension. *Biomaterials* **2011**, 32, 2256–2264.
- (13) Wang, L.-S.; Boulaire, J.; Chan, P. P. Y.; Chung, J. E.; Kurisawa, M. The role of stiffness of gelatin—hydroxyphenylpropionic acid hydrogels formed by enzyme-mediated crosslinking on the differentiation of human mesenchymal stem cell. *Biomaterials* **2010**, *31*, 8608–8616.
- (14) Burke, G.; Devine, D. M.; Major, I. Effect of Stereolithography 3D Printing on the Properties of PEGDMA Hydrogels. *Polymers* **2020**, *12*, 2015.
- (15) Lin, C.-C.; Sawicki, S. M.; Metters, A. T. Free-Radical-Mediated Protein Inactivation and Recovery during Protein Photoencapsulation. *Biomacromolecules* **2008**, *9*, 75–83.
- (16) McCall, J. D.; Anseth, K. S. Thiol—Ene Photopolymerizations Provide a Facile Method To Encapsulate Proteins and Maintain Their Bioactivity. *Biomacromolecules* **2012**, *13*, 2410–2417.
- (17) Genidy, M. S.; Madhukar, M. S.; Russell, J. D. A New Method to Reduce Cure-Induced Stresses in Thermoset Polymer Composites, Part II: Closed Loop Feedback Control System. *J. Compos. Mater.* **2000**, *34*, 1905–1925.
- (18) Kurtz, M. J.; Guang-Yan, Z.; Henson, M. A. Constrained output feedback control of a multivariable polymerization reactor. *IEEE Trans. Control Syst. Technol.* **2000**, *8*, 87–97.
- (19) Zhao, X.; Rosen, D. W. An implementation of real-time feedback control of cured part height in Exposure Controlled

- Projection Lithography with in-situ interferometric measurement feedback. *Addit. Manuf.* **2018**, 23, 253–263.
- (20) Buxton, A. N.; Zhu, J.; Marchant, R.; West, J. L.; Yoo, J. U.; Johnstone, B. Design and Characterization of Poly(Ethylene Glycol) Photopolymerizable Semi-Interpenetrating Networks for Chondrogenesis of Human Mesenchymal Stem Cells. *Tissue Eng.* **2007**, *13*, 2549–2560.
- (21) Bahney, C. S.; Lujan, T. J.; Hsu, C. W.; Bottlang, M.; West, J. L.; Johnstone, B. Visible light photoinitiation of mesenchymal stem cell-laden bioresponsive hydrogels. *Eur. Cells Mater.* **2011**, 22, 43–55.
- (22) Burke, G.; Barron, V.; Geever, T.; Geever, L.; Devine, D. M.; Higginbotham, C. L. Evaluation of the materials properties, stability and cell response of a range of PEGDMA hydrogels for tissue engineering applications. *J. Mech. Behav. Biomed. Mater.* **2019**, *99*, 1–10
- (23) Cui, X.; Breitenkamp, K.; Finn, M. G.; Lotz, M.; D'Lima, D. D. Direct Human Cartilage Repair Using Three-Dimensional Bioprinting Technology. *Tissue Eng., Part A* **2012**, *18*, 1304–1312.
- (24) Ferguson, C. T. J.; Huber, N.; Landfester, K.; Zhang, K. A. I. Dual-Responsive Photocatalytic Polymer Nanogels. *Angew. Chem., Int. Ed.* **2019**, *58*, 10567–10571.
- (25) Weda, P.; Trzebicka, B.; Dworak, A.; Tsvetanov, C. B. Thermosensitive nanospheres of low-density core An approach to hollow nanoparticles. *Polymer* **2008**, *49*, 1467–1474.
- (26) Sharma, H.; Lakshmanan, R. S.; Johnson, B. N.; Mutharasan, R. Piezoelectric cantilever sensors with asymmetric anchor exhibit picogram sensitivity in liquids. *Sens. Actuators, B* **2011**, *153*, 64–70.
- (27) Haring, A. P.; Khan, A. U.; Liu, G.; Johnson, B. N. 3D Printed Functionally Graded Plasmonic Constructs. *Adv. Opt. Mater.* **2017**, *5*, 1700367.
- (28) Haring, A. P.; Thompson, E. G.; Tong, Y.; Laheri, S.; Cesewski, E.; Sontheimer, H.; Johnson, B. N. Process- and bio-inspired hydrogels for 3D bioprinting of soft free-standing neural and glial tissues. *Biofabrication* **2019**, *11*, No. 025009.
- (29) Haring, A. P.; Tong, Y.; Halper, J.; Johnson, B. N. Programming of Multicomponent Temporal Release Profiles in 3D Printed Polypills via Core–Shell, Multilayer, and Gradient Concentration Profiles. *Adv. Healthcare Mater.* **2018**, *7*, 1800213.
- (30) Moran, M. B.; Martin, G. C. The Laser Raman Spectrum of Polyethylene Glycol Dimethacrylate. *J. Macromol. Sci., Part A: Chem.* 1983, 19, 611–618.
- (31) Bäckström, S.; Benavente, J.; Berg, R. W.; Stibius, K.; Larsen, M. S.; Bohr, H.; Hélix-Nielsen, C. Tailoring Properties of Biocompatible PEG-DMA Hydrogels with UV Light. *Mater. Sci. Appl.* **2012**, *03*, 7.
- (32) Wang, L.; Zhao, X.; Zhang, Y.; Zhang, W.; Ren, T.; Chen, Z.; Wang, F.; Yang, H. Fabrication of intelligent poly(N-isopropylacry-lamide)/silver nanoparticle composite films with dynamic surface-enhanced Raman scattering effect. RSC Adv. 2015, 5, 40437–40443.
- (33) Cesewski, E.; Singh, M.; Liu, Y.; Zhang, J.; Haring, A. P.; Johnson, B. N. Real-time monitoring of hydrogel rheological property changes and gelation processes using high-order modes of cantilever sensors. *J. Appl. Phys.* **2020**, *128*, 174502.
- (34) Haring, A. P.; Singh, M.; Koh, M.; Cesewski, E.; Dillard, D. A.; Kong, Z. J.; Johnson, B. N. Real-time characterization of hydrogel viscoelastic properties and sol-gel phase transitions using cantilever sensors. *J. Rheol.* **2020**, *64*, 837–850.
- (35) Killion, J. A.; Geever, L. M.; Devine, D. M.; Kennedy, J. E.; Higginbotham, C. L. Mechanical properties and thermal behaviour of PEGDMA hydrogels for potential bone regeneration application. *J. Mech. Behav. Biomed. Mater.* **2011**, *4*, 1219–1227.
- (36) Zheng, W. J.; An, N.; Yang, J. H.; Zhou, J.; Chen, Y. M. Tough Al-alginate/Poly(N-isopropylacrylamide) Hydrogel with Tunable LCST for Soft Robotics. ACS Appl. Mater. Interfaces 2015, 7, 1758–1764.
- (37) Warren, H.; in het Panhuis, M.; Spinks, G. M.; Officer, D. L. Thermal actuation of hydrogels from PNIPAm, alginate, and carbon nanofibres. *J. Polym. Sci., Part B: Polym. Phys.* **2018**, *56*, 46–52.

- (38) Zhang, H.; Zhang, Y.; He, L.; Yang, B.; Zhu, S.; Yao, M. Thermal-responsive poly(N-isopropyl acrylamide)/sodium alginate hydrogels: preparation, swelling behaviors, and mechanical properties. *Colloid Polym. Sci.* **2016**, 294, 1959–1967.
- (39) Johnson, B. N.; Mutharasan, R. Persistence of bending and torsional modes in piezoelectric-excited millimeter-sized cantilever (PEMC) sensors in viscous liquids 1 to 103 cP. *J. Appl. Phys.* **2011**, *109*, No. 066105.
- (40) Andrzejewska, E. Photopolymerization kinetics of multifunctional monomers. *Prog. Polym. Sci.* **2001**, *26*, 605–665.
- (41) Zandvliet, M. J.; Bosgra, O. H.; Jansen, J. D.; Van den Hof, P. M. J.; Kraaijevanger, J. F. B. M. Bang-bang control and singular arcs in reservoir flooding. *J. Pet. Sci. Eng.* **2007**, *58*, 186–200.
- (42) Zuyev, A.; Seidel-Morgenstern, A.; Benner, P. An isoperimetric optimal control problem for a non-isothermal chemical reactor with periodic inputs. *Chem. Eng. Sci.* **2017**, *161*, 206–214.
- (43) Smets, U. Y.; Dochain, D.; Impe, J. F. V. Optimal spatial temperature control of a steady-state exothermic plug flow reactor. Part I: Bang-bang control; 2001 European Control Conference (ECC), 4–7 Sept. 2001; 2001; pp. 2540–2545.
- (44) Smets, I. Y.; Claes, J. E.; November, E. J.; Bastin, G. P.; Van Impe, J. F. Optimal adaptive control of (bio)chemical reactors: past, present and future. *J. Process Control* **2004**, *14*, 795–805.
- (45) Johnson, B. N.; Mutharasan, R. Biosensing using dynamic-mode cantilever sensors: A review. *Biosens. Bioelectron.* **2012**, 32, 1–18
- (46) Ziegler, C. Cantilever-based biosensors. Anal. Bioanal. Chem. 2004, 379, 946-959.
- (47) Kizilay, M. Y.; Okay, O. Effect of hydrolysis on spatial inhomogeneity in poly(acrylamide) gels of various crosslink densities. *Polymer* **2003**, *44*, 5239–5250.
- (48) Patras, G.; Qiao, G. G.; Solomon, D. H. Controlled Formation of Microheterogeneous Polymer Networks: Influence of Monomer Reactivity on Gel Structure. *Macromolecules* **2001**, *34*, 6396–6401.
- (49) Burke, G.; Cao, Z.; Devine, D. M.; Major, I. Preparation of Biodegradable Polyethylene Glycol Dimethacrylate Hydrogels via Thiol-ene Chemistry. *Polymer* **2019**, *11*, 1339.
- (50) Lee, S.; Tong, X.; Yang, F. Effects of the poly(ethylene glycol) hydrogel crosslinking mechanism on protein release. *Biomater. Sci.* **2016**, *4*, 405–411.
- (51) Axpe, E.; Chan, D.; Offeddu, G. S.; Chang, Y.; Merida, D.; Hernandez, H. L.; Appel, E. A. A Multiscale Model for Solute Diffusion in Hydrogels. *Macromolecules* **2019**, *52*, 6889–6897.
- (52) Fang, N.; Sun, C.; Zhang, X. Diffusion-limited photopolymerization in scanning micro-stereolithography. *Appl. Phys. A: Mater. Sci. Process.* **2004**, *79*, 1839–1842.
- (53) Ranganathan, N.; Joseph Bensingh, R.; Abdul Kader, M.; Nayak, S. K. Synthesis and Properties of Hydrogels Prepared by Various Polymerization Reaction Systems. In *Cellulose-Based Superabsorbent Hydrogels*; Mondal, M. I. H., Ed.; Springer International Publishing: Cham, 2018; pp. 1–25.
- (54) Olejniczak, M. N.; Kozanecki, M.; Saramak, J.; Matusiak, M.; Kadlubowski, S.; Matyjaszewski, K. Raman spectroscopy study on influence of network architecture on hydration of poly(2-(2-methoxyethoxy)ethyl methacrylate) hydrogels. *J. Raman Spectrosc.* **2017**, *48*, 465–473.
- (55) Yu, D.; Huang, R.; Knox, W. H. Femtosecond laser micromachining in ophthalmic hydrogels: spectroscopic study of materials effects. *Opt. Mater. Express* **2019**, *9*, 3292–3305.
- (56) Roffel, B.; Chin, P. A. Application of fuzzy logic in the control of polymerization reactors. *Control Eng. Pract.* **1993**, *1*, 267–272.
- (57) Lima, N. M. N.; Liñan, L. Z.; Filho, R. M.; Maciel, M. R. W.; Embiruçu, M.; Grácio, F. Modeling and predictive control using fuzzy logic: Application for a polymerization system. *AIChE J.* **2010**, *56*, 965–978.
- (58) Corrigan, N.; Yeow, J.; Judzewitsch, P.; Xu, J.; Boyer, C. Seeing the Light: Advancing Materials Chemistry through Photopolymerization. *Angew. Chem., Int. Ed.* **2019**, *58*, 5170–5189.

- (59) Konkolewicz, D.; Schröder, K.; Buback, J.; Bernhard, S.; Matyjaszewski, K. Visible Light and Sunlight Photoinduced ATRP with ppm of Cu Catalyst. *ACS Macro Lett.* **2012**, *1*, 1219–1223.
- (60) Xu, J.; Jung, K.; Atme, A.; Shanmugam, S.; Boyer, C. A Robust and Versatile Photoinduced Living Polymerization of Conjugated and Unconjugated Monomers and Its Oxygen Tolerance. *J. Am. Chem. Soc.* **2014**, *136*, 5508–5519.
- (61) McKenzie, T. G.; Colombo, E.; Fu, Q.; Ashokkumar, M.; Qiao, G. G. Sono-RAFT Polymerization in Aqueous Medium. *Angew. Chem., Int. Ed.* **2017**, *56*, 12302–12306.